Supporting Information

Confinement Effects and Charge Dynamics in Zn_3N_2 Colloidal Quantum Dots: Implications for QD-LED displays.

Ruben Ahumada-Lazo[1], Simon M. Fairclough[2‡], Samantha J. O. Hardman[3], Peter N. Taylor[4], Mark Green[5], Sarah J. Haigh[2], Rinku Saran[6†], Richard J. Curry[6] and David J. Binks[1*].

[1]Department of Physics and Astronomy and the Photon Science Institute, [2]Department of Materials, [3]Manchester Institute of Biotechnology, The University of Manchester, Manchester, M13 9PL, [4]Sharp Laboratories of Europe Ltd, Edmund Halley Road, Oxford Science Park, Oxford, OX4 4GB, UK, [5]Department of Physics, King's College London, Strand, London, UK WC2R 2LS. [6]Photon Science Institute, Department of Electrical and Electronic Engineering, The University of Manchester, Manchester, M13 9PL, United Kingdom.
Present addresses:
[‡]Cambridge Centre for Gallium Nitride, University of Cambridge, Cambridge, CB3 0FS, United Kingdom, [†]NanoScience Technology Center, University of Central Florida, Orlando, Florida 32826, USA.

*Authors to whom correspondence should be addressed, electronic email: david.binks@manchester.ac.uk

S1. TEM images and size frequency histograms

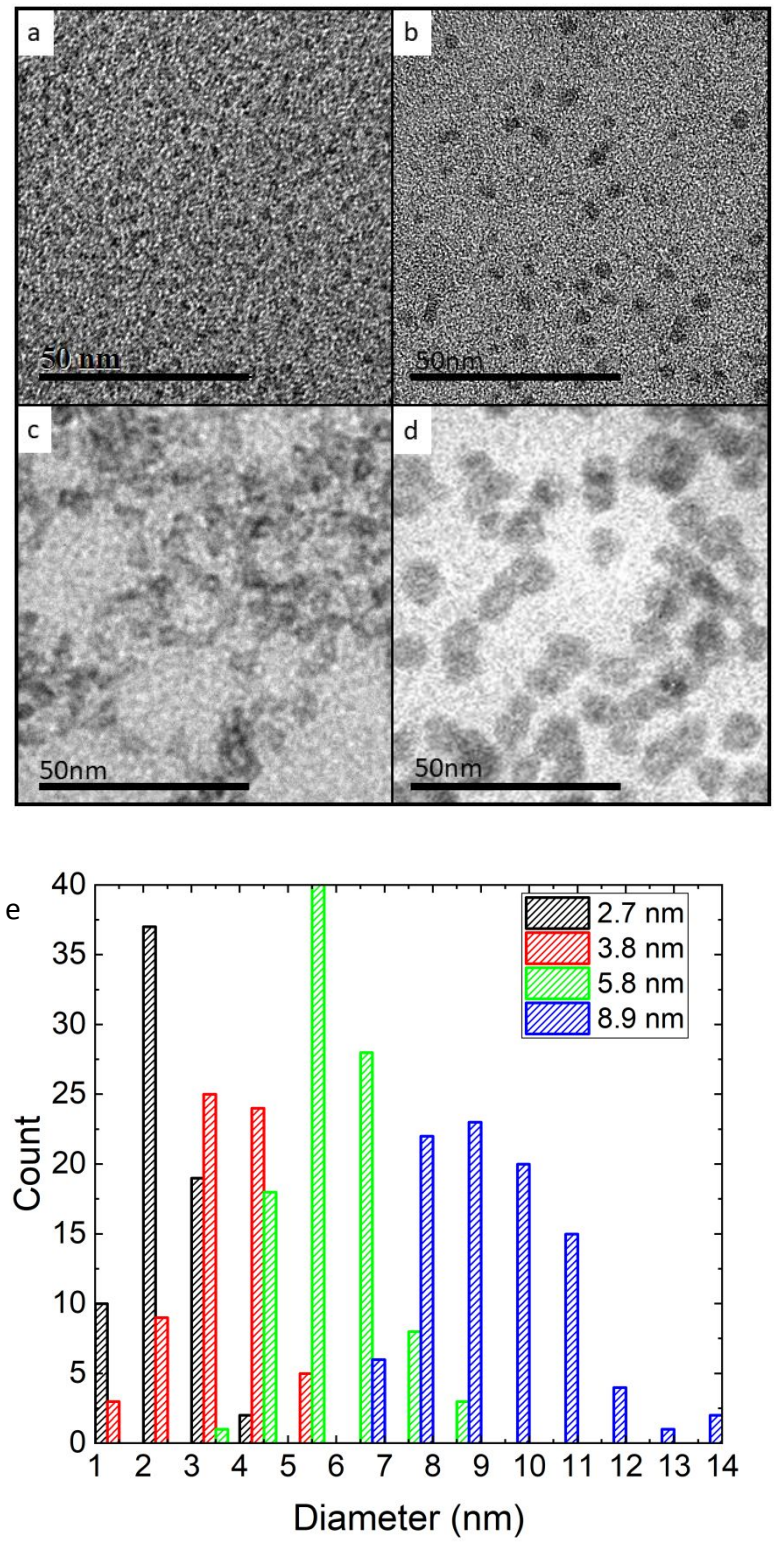

Figure S1. TEM images of Zn_3N_2 samples with average diameters, D, of a) 2.7 nm b) 3.8 nm, c) 5.8 nm and d) 8.9 nm. e) Size frequency histograms of the Zn_3N_2 samples. The standard deviations of the size distribution for each sample are 23%, 20%, 17% and 18%, respectively.

S2. Second derivative of the absorption spectra.

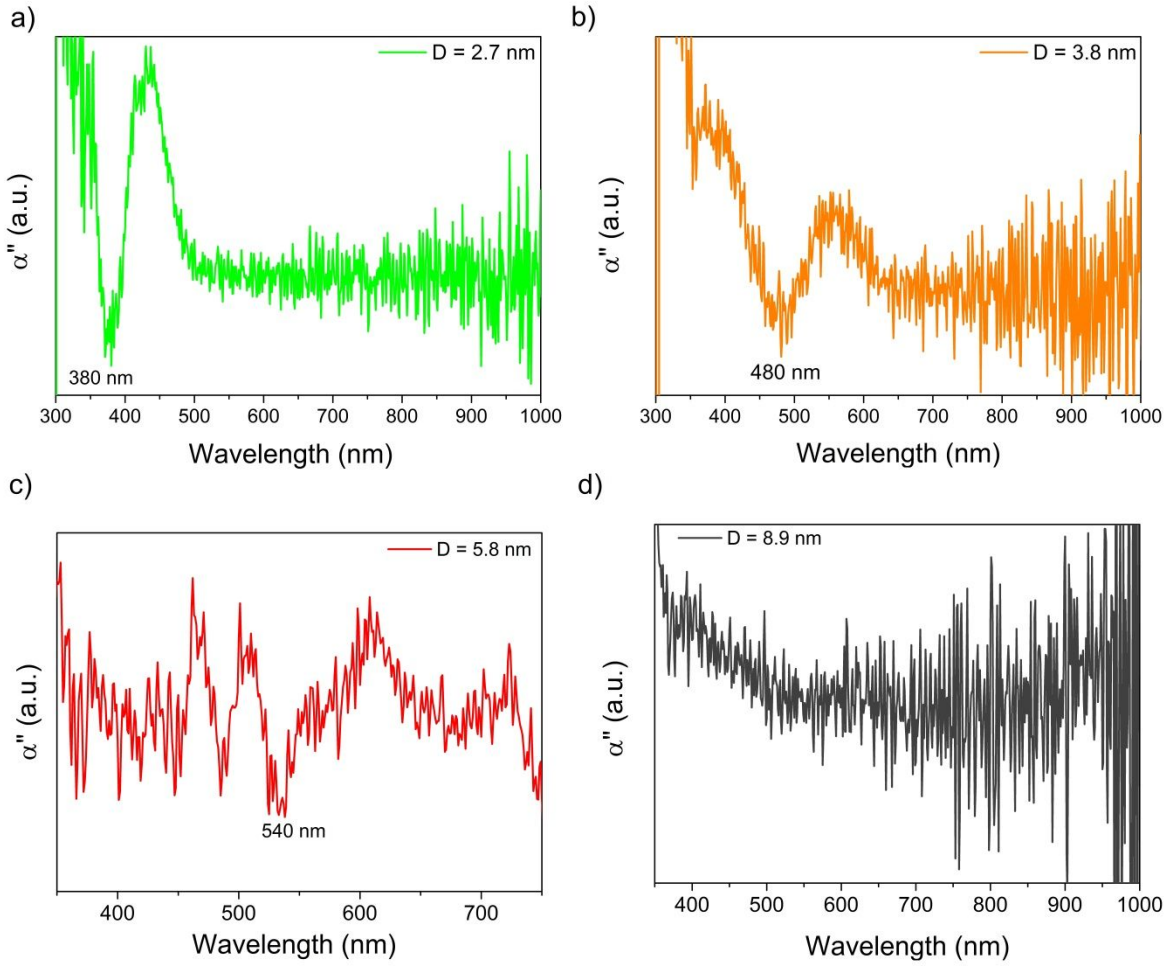

Figure S2. Second derivative $\alpha^{"}$ of the steady-state absorption spectra for samples with average diameters of a) 2.7 nm, b) 3.8 nm, c) 5.8 nm and d) 8.9 nm.

Table S1. Dielectric constant and effective masses found in literature

Dielectric constant $\in_r$	**Electron effective mass** m_e	**Hole effective mass** m_h
5.29 [1] 2.89 – 5.76 [2] 5.29 – 7.29 [3]	$0.29m_o$ [1,4] $0.27m_o$ [5] $0.08m_o$ [6,7]	$0.99m_o$ [6]

Where m_o = 9.109 x 10^{-31} kg is the electron rest mass

S3. Transient absorption spectra.

The contour plots of the pump-induced absorption change, ΔA, spectra as a function of delay time, obtained at excitation fluences from ~ 1.1 x 10^{14} to ~ 3.4 x 10^{15} photons·cm^{-2} for samples with average QD diameters of 3.8 nm, 5.8 nm and 8.9 nm are shown in figures S3, S4 and S5, respectively. As discussed in the main text, the main feature in the plots for sample with 3.8 nm average diameter (figure S3) is a strong bleach signal (negative ΔA) centered at around 500 nm. For the case of the samples with QD diameters of 5.8 nm and 8.9 nm, the bleach peaks are centered at approximately 560 nm and 840 nm, respectively.

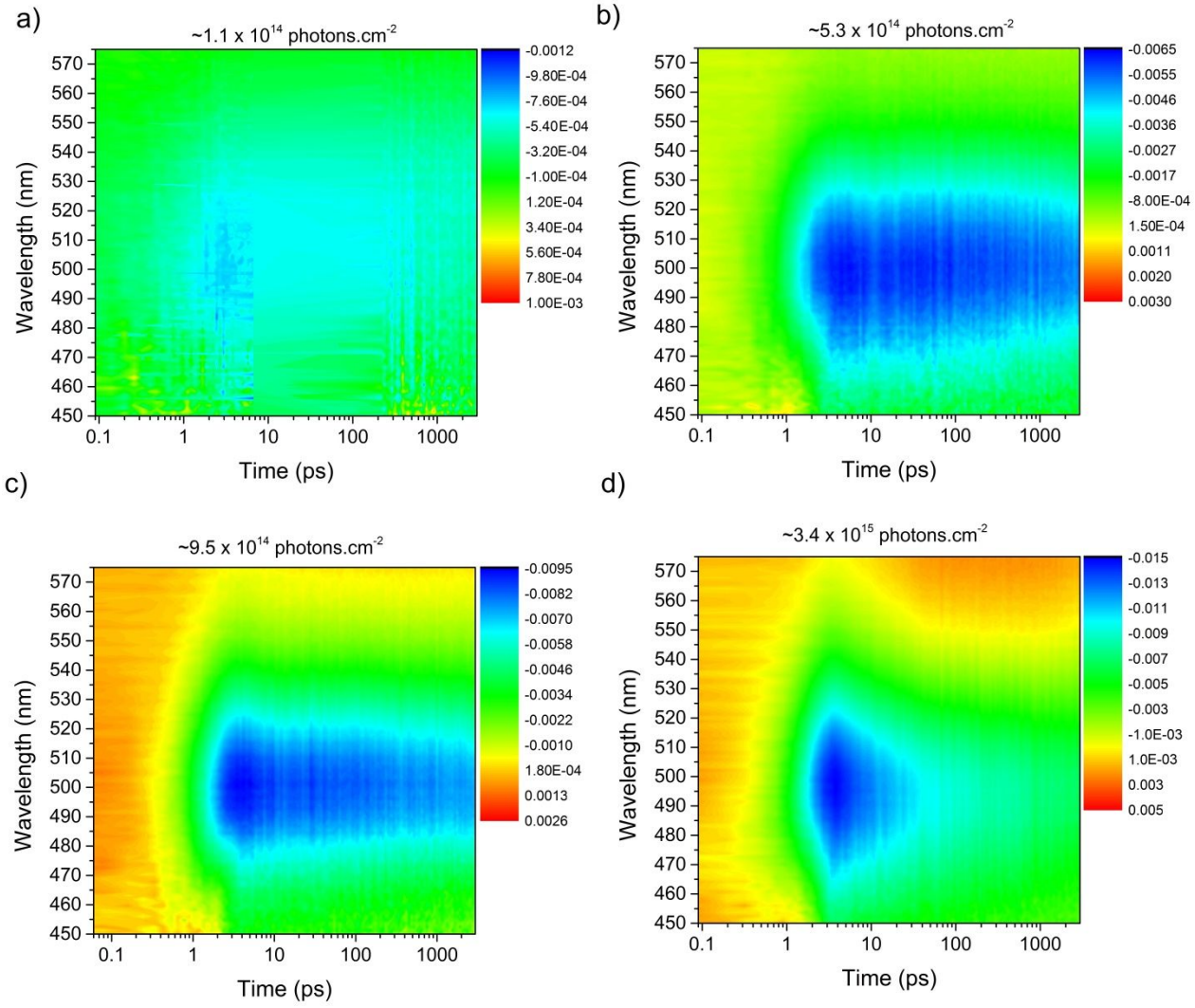

Figure S3 a-d). Contour plots of the change in absorption, ΔA (in OD), as a function of wavelength and delay time recorded at different excitation fluence for sample with 3.8 nm average diameter.

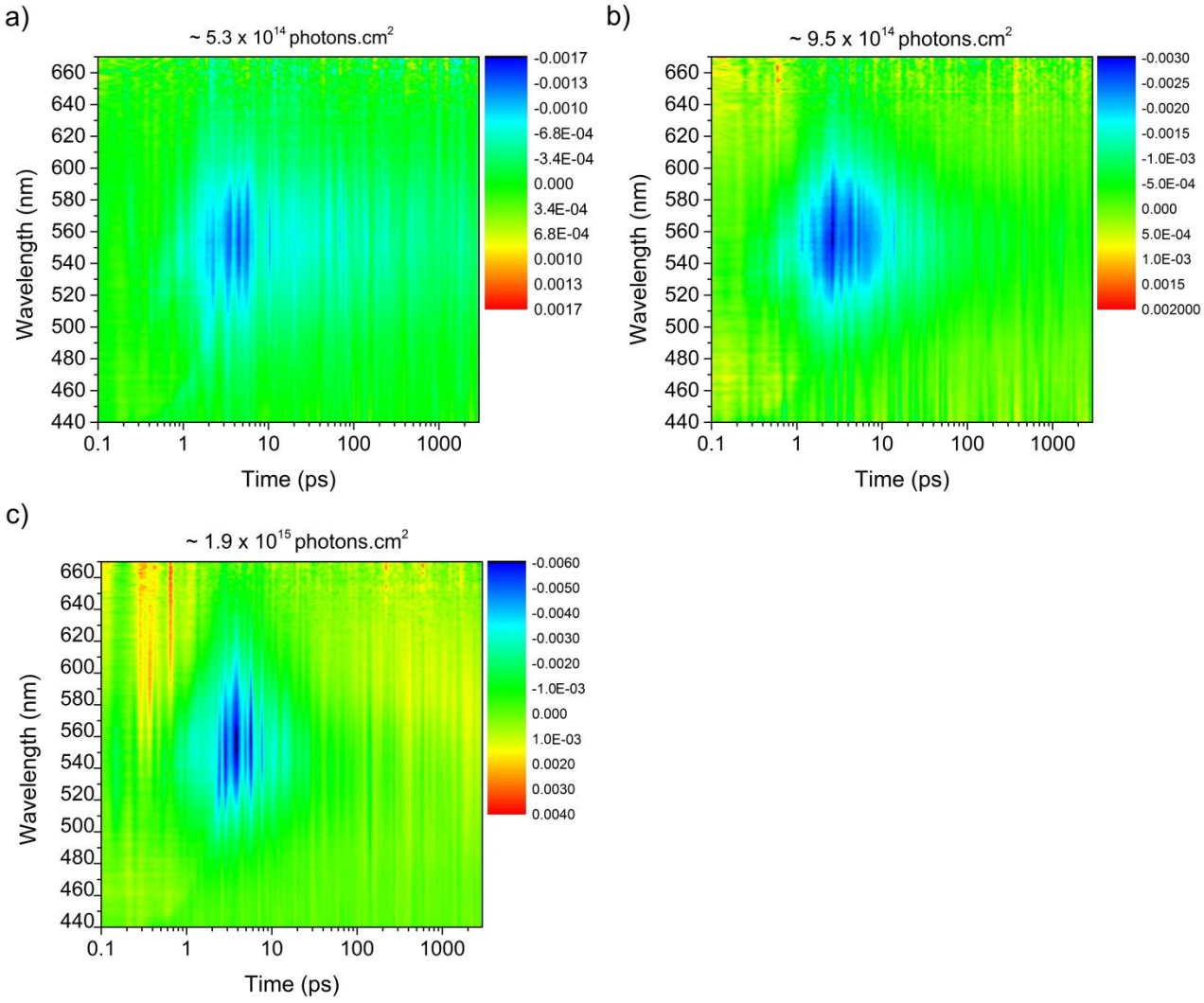

Figure S4 a-c). Contour plots of the change in absorption, ΔA (in OD), as a function of wavelength and delay time recorded at different excitation fluence for sample with 5.8 nm average diameter.

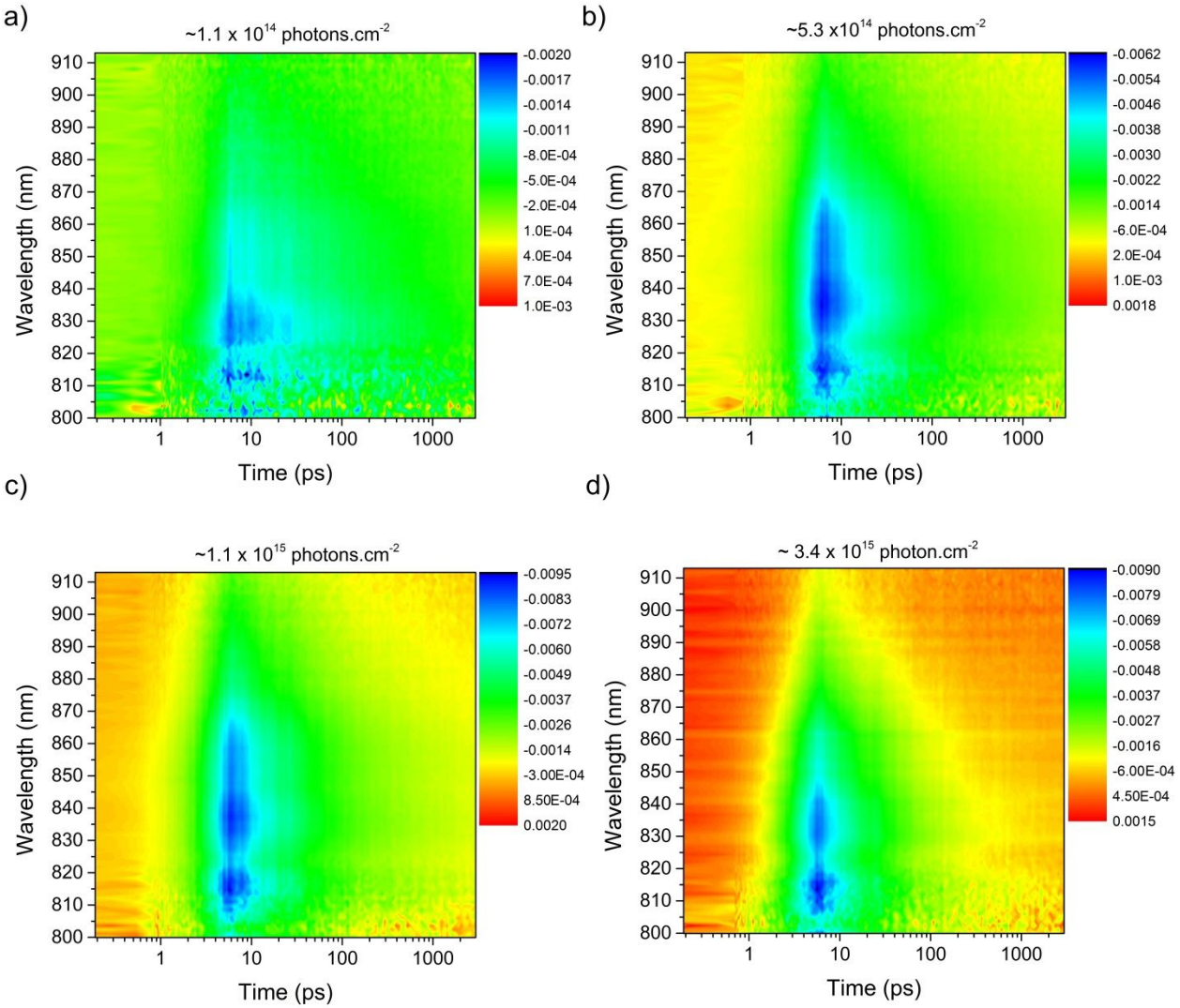

Figure S5 a-d). Contour plots of the change in absorption, ΔA (in OD), as a function of wavelength and delay time recorded at different excitation fluence for sample with 8.9 nm average diameter.

Figure S6 shows the maximum fractional bleach, $\Delta A/A$, at the wavelengths of the CBM as a function of excitation fluence, J_p, for samples with 5.8 nm and 8.9 nm average diameters. A two-fold degeneracy and an absorption cross-section, σ, of 1.3 ± 0.3 x 10^{-15} cm^2 and 2.04 ± 0.03 x 10^{-15} cm^2 were determined for these samples, respectively as detailed in the main text.

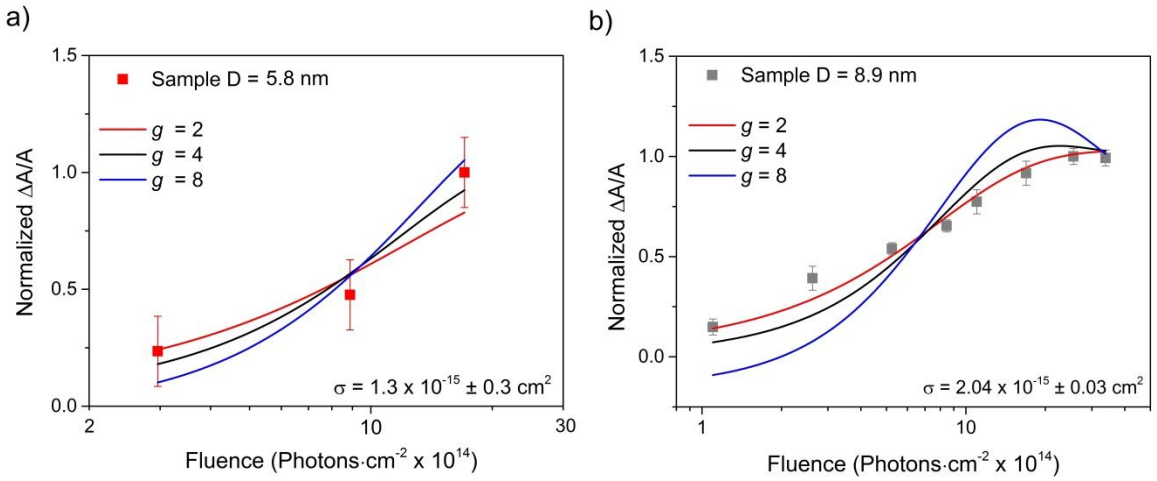

Figure S6. Normalized ΔA/A as a function of excitation fluence for samples with a) 4.5 nm and b) 8.9 nm average diameters. Fits are to equation (1) presented in the main text.

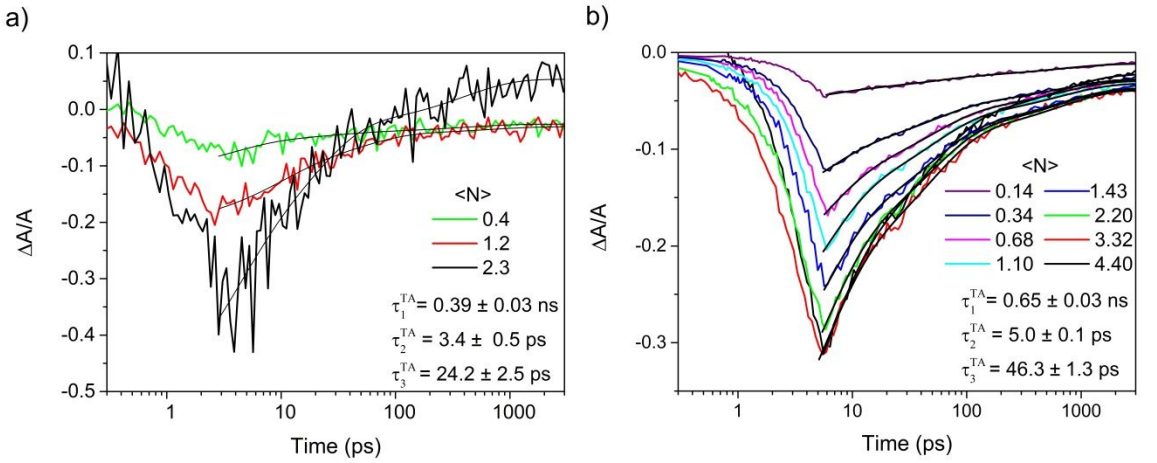

Figure S7. Fractional absorption change $\Delta A/A$ transients at different excitation fluences ($\langle N \rangle$) for the samples with a) 5.8 nm and b) 8.9 nm average diameters. Tri-exponential fits to the decays are shown as black lines.

S3. Transient photoluminescence measurements.

The PL decay transients obtained with an excitation pulse of 420 nm and detecting at the PL emission peak of the samples with average diameters of 2.7 nm and 3.8 nm are shown in figure S8. Both transients are well described by a tri-exponential decay function of the form $\tau_{PL} = y_0 + A_1 e^{-x/\tau_1} + A_2 e^{-x/\tau_2} + A_3 e^{-x/\tau_3}$, where y_0 is an offset, $\tau_i^{PL} (i = 1, 2, 3)$ are the time constants and A_i are their corresponding amplitudes. The shortest of these time constants, τ_1^{PL} for the sample with average diameter of 3.8 nm corresponds to the longest extracted from the TA measurements and identified as the lifetime of single excitons, τ_1^{TA}.

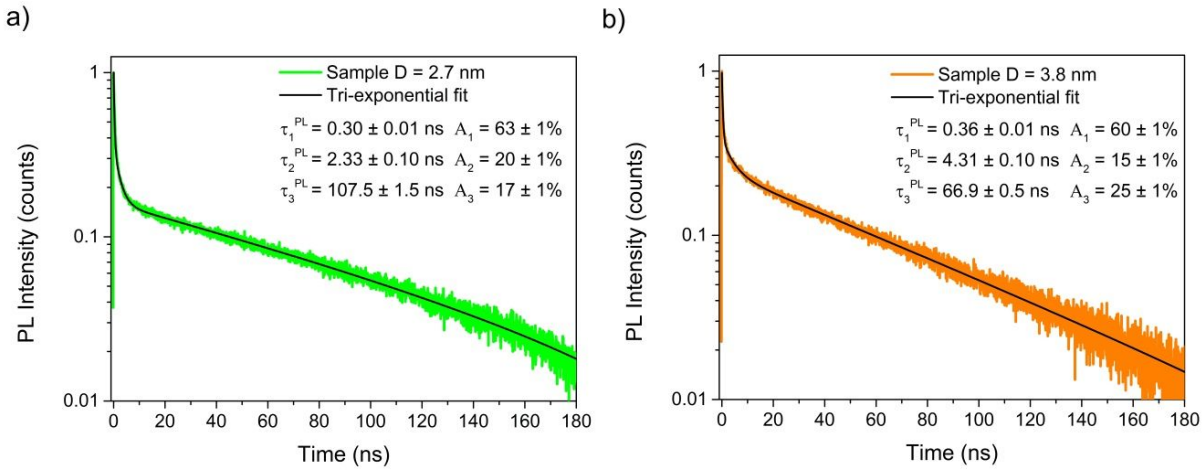

Figure S8. PL decays for samples with average diameters of a) 2.7 nm and b) 3.8 nm. Tri-exponential fits to the decays are shown as black lines.

S4 Band gap as a function of size

The values for band gap estimated from the second derivative of the absorbance are plotted as a function of the QD diameter in figure S9. These experimental data were fitted by the equation:

$$E_{\mathrm{g}}(NC) = E_{\mathrm{g}}(bulk) + \left(\frac{\pi^2\hbar^2}{2m_r R^2}\right) - \frac{1}{\varepsilon_r^2}\frac{m_r}{m_0}R_y,$$

where m_r is the reduced mass, $m_r = (m_e^{-1} + m_h^{-1})^{-1}$, R is the QDs radius, $\varepsilon_r$is the dielectric constant and R_y is Rydberg's energy. The values of electron effective mass, band gap and dielectric constant were set as experimentally measured values form the literature [1,3,4] and are given in the figure. The value for hole effective mass was left to vary since no experimental values for it have yet been reported.

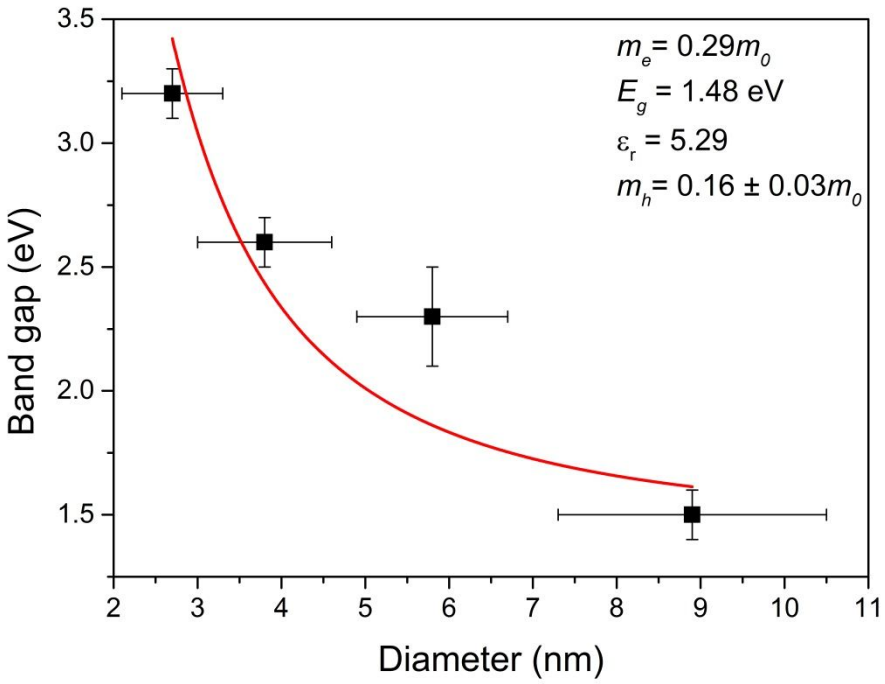

Figure S9. Band gap plotted as a function of diameter for Zn_3N_2 QD samples. The red line is the fit to the effective mass model shown above.

S5 Vibrational coupling

A Fast Fourier Transform (FFT) was performed on some representative TA decays to explore the possibility of exciton-phonon coupling in Zn_3N_2. As can be seen in figure S10, in all cases there is only one feature close to frequency values of zero, arising from the limited time window of the transient absorption experiments. No features indicating exciton coupling with either optical or acoustic phonons (such as those observed for CdSe QDs [8]), can be seen.

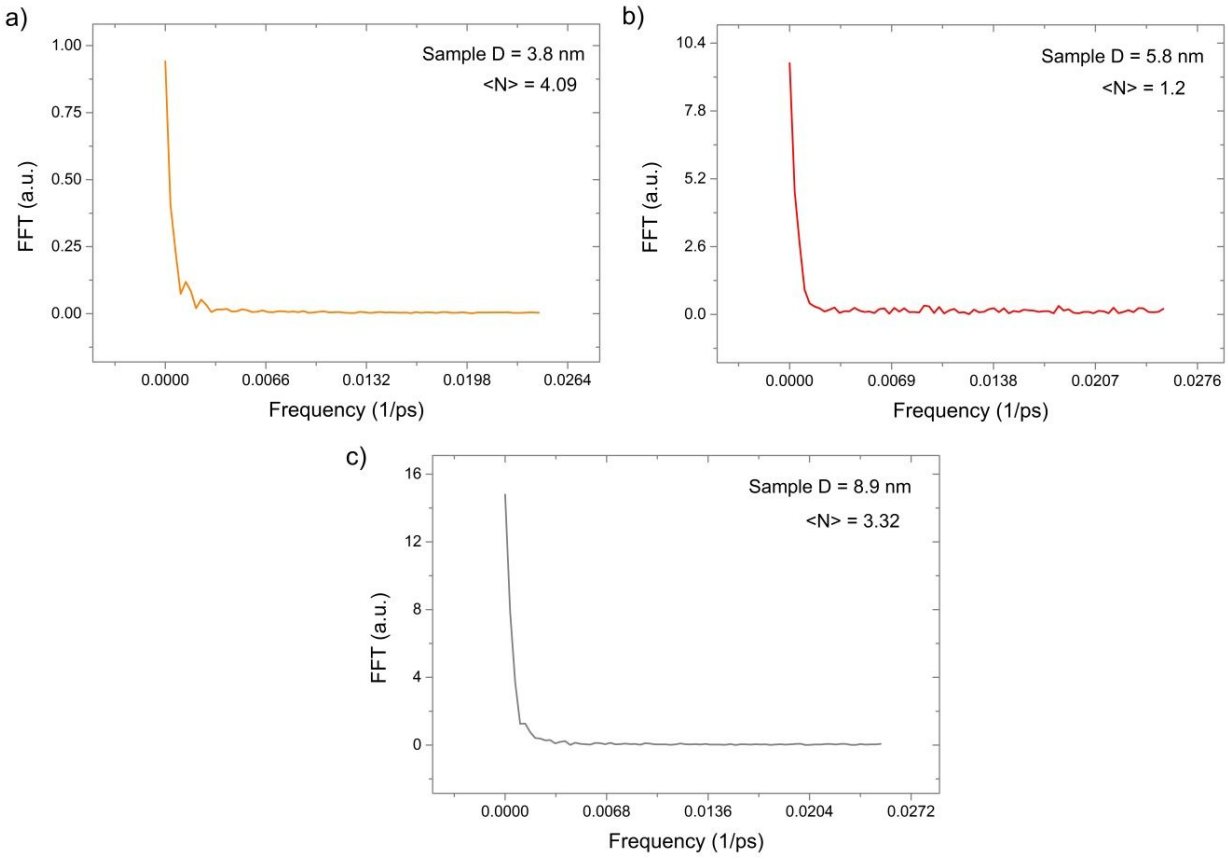

Figure S10. Fourier transform for selected fractional absorption change transients for Zn_3N_2 samples a) D = 3.8 nm, b) D = 5.8 nm and c) D = 8.9 nm. No features indicating exciton-phonon coupling are observed.

References

(1) Zervos, M.; Karipi, C.; Othonos, A. Zn3N2 Nanowires: Growth, Properties and Oxidation. *Nanoscale Res. Lett.* **2013**, *56* (8), 4914–4919.

(2) Ayouchi, R.; Casteleiro, C.; Santos, L.; Schwarz, R. RF-Plasma Assisted PLD Growth of Zn3N2 Thin Films. *Phys. Status Solidi Curr. Top. Solid State Phys.* **2010**, *7* (9), 2294–2297.

(3) Trapalis, A.; Heffernan, J.; Farrer, I.; Sharman, J.; Kean, A. Structural, Electrical, and Optical Characterization of as Grown and Oxidized Zinc Nitride Thin Films. *J. Appl. Phys.* **2016**, *120* (20), 205102 1-9.

(4) Suda, T.; Kakishita, K. Band-Gap Energy and Electron Effective Mass of Polycrystalline Zn3N2. *J. Appl. Phys.* **2006**, *99* (7), 1–4.

(5) Yamada, N.; Watarai, K.; Yamaguchi, T.; Sato, A.; Ninomiya, Y. Transparent Conducting Zinc Nitride Films. *Jpn. J. Appl. Phys.* **2014**, *53* (5 SPEC. ISSUE 1), 05FX01 1-5.

(6) Kumagai, Y.; Harada, K.; Akamatsu, H.; Matsuzaki, K.; Oba, F. Carrier-Induced Band-Gap Variation and Point Defects in Zn3N2 from First Principles. *Phys. Rev. Appl.* **2017**, *8* (1), 27–30.

(7) Cao, X.; Yamaguchi, Y.; Ninomiya, Y.; Yamada, N. Comparative Study of Electron Transport Mechanisms in Epitaxial and Polycrystalline Zinc Nitride Films. *J. Appl. Phys.* **2016**, *119* (2), 025104 1-10.

(8) Sagar, D. M.; Cooney, R. R.; Sewall, S. L.; Kambhampati, P. State-Resolved Exciton-Phonon Couplings in CdSe Semiconductor Quantum Dots. *J. Phys. Chem. C* **2008**, *112* (25), 9124–9127.